Wavelength-Scale Focusing Transducer Based on Suspended Aluminum Nitride Thin Film

Jiawei Li[1,2,3], Lihui Jin[1], Mingye Du[1,2,3], Peng Wu[5], Yitao Liao[5], Tao Wu[1,2,3,4*]
[1]School of Information Science and Technology, ShanghaiTech University, Shanghai, 201210, China
[2]Shanghai Institute of Microsystem and Information Technology,
Chinese Academy of Sciences, Shanghai, 200050, China
[3]University of Chinese Academy of Sciences, Beijing, 100049, China
[4]Shanghai Engineering Research Center of Energy Efficient and Custom AI IC, Shanghai, 201210, China
[5]Xuzhou Liyu Advanced Technology Co. Ltd., Xuzhou, Jiangsu, China

***Abstract*—A wavelength-scale focusing transducer based on suspended Aluminum nitride (AlN) piezoelectric thin film are designed, simulated and fabricated. The one port device was simulated and analyzed to verify the device focusing performance. Two-port acoustic delay line under different electrical configuration was simulated, fabricated and analyzed to evaluate the electro-acoustic transduction capability of the transducer. According to the simulation and measurenment results, the transducer can produce the expected focused gaussian lamb beam with a beam waist of 5 μm which is half of the wavelength. The insertion loss of 32.16 dB at 824.13 MHz proves the efficient electromechanical transduction capability of the transducer. The transducer is the potential component in phononic integrated circuits (PnICs).**

***Index Terms*—Aluminum nitride, Phononic Integrated Circuit, Gaussian Acoustics**

I. Introduction

Phononic integrated circuits (PnICs) is an emerging field that aims to manipulate and control phonons in a manner analogous to how electronic integrated circuits handle electrons. Compared with electromagnetic waves, acoustic waves in solids have lower velocity and loss, enabling effective signal processing with a smaller size. In addition, acoustic waves in solids do not radiate into free space, so crosstalk from other devices and the environment can be effectively attenuated. Acoustic devices have been widely used in signal processing and sensing. By utilizing wavelength size structures, phononic circuits are able to limit the number of modes in the system, offering control over factors such as loss and coupling. This enhanced control over wave behavior allows for the efficient processing and routing of signals through the circuit, resulting in improved performance and functionality [1]. However, the current control level of phonon is far from their counterparts photons and electrons. Photonic integrated circuits enable the integration of optical components on chip to achieve optical systems with unprecedented performance [2]. This is largely achieved by highly constrained waveguides that are compact, allow for tight bending, and concentrate energy into a small mode region for efficient interactions. However, a similar function does not yet apply to phonon circuits. The ability to focus and couple acoustic wave to wavelength-scale waveguide needs to be further explored.

In order to persue the mode control ability, wavelength-scale structures are used to routing acoustic wave [3]. The development of modern micro/nano manufacturing technology accelerates the research of phonon integrated circuit. In prior efforts to effectively stimulate a wavelength-scale waveguide, researchers have employed techniques such as designing the transducer to concentrate the emission [4], or implementing a tapered interface between the waveguide and transducer [5]. Transducers that produce Gaussian Lamb wave beams in thin aluminum nitride membranes was fabricated to excite wavelength-scale structures [6]. Amirparsa et al. realized single mode waveguide of single phonon in suspended silicon microstructure [7]. Complete on-chip control of a single phonon strongly restricted along the propagation axis is shown. Fu et al. established the architecture of phonon integrated circuits on GaN/sapphire semiconductor substrates. Low loss single mode strip waveguide and coupled high Q ring resonator are presented to demonstrate the basic functions of phonon circuit [8].

Currently, phonon circuits have been developed on several platforms, including suspended [9] or unreleased ridge waveguides [10]. These devices show outstanding progress in the miniaturization of acoustic waveguide structure and the design of band structure of waveguide, which contributed to the development of phonon integrated circuit. In order to further realize the potential of phonon integrated circuits, this paper aims to explore a platform that combines small area and efficient electromechanical conversion with miniaturized acoustic waveguide, which shows high conduction constraint capability to realize effective control of phonons for information processing.

II. Design and Simulation

The suspended structure based on AlN thin film was simulated and analyzed by finite element analysis (FEA) simulations. The simulation model is shown in Fig. 1(a). Low reflection boundary are added to the boundary of the model to reduce the influence of significantly reflecting wave. The cross section view is shown in Fig. 1(b). Three layers are respectively the 100 nm platinum bottom electrode, 1 μm AlN piezoelectric film and 100 nm platinum focusing

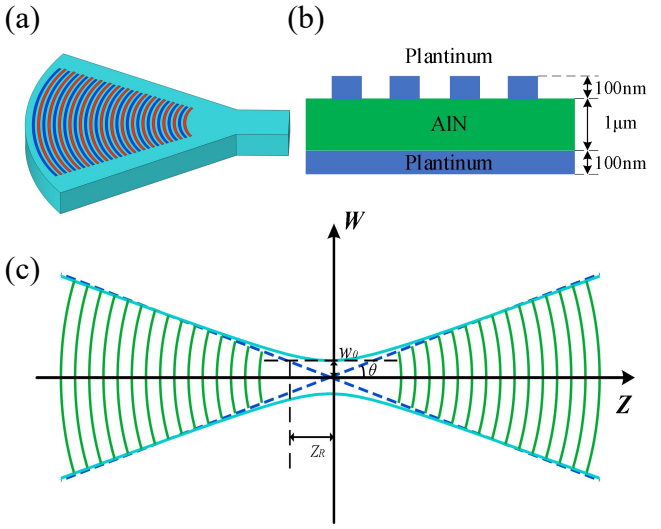

Fig. 1. (a) Schematic of the simulation model. (b) Cross section view of the model. (c) The position of electrodes which is fitted to the wavefront of Gaussian wave, the first electrode finger starts at 5 wavelengths from the focal point.

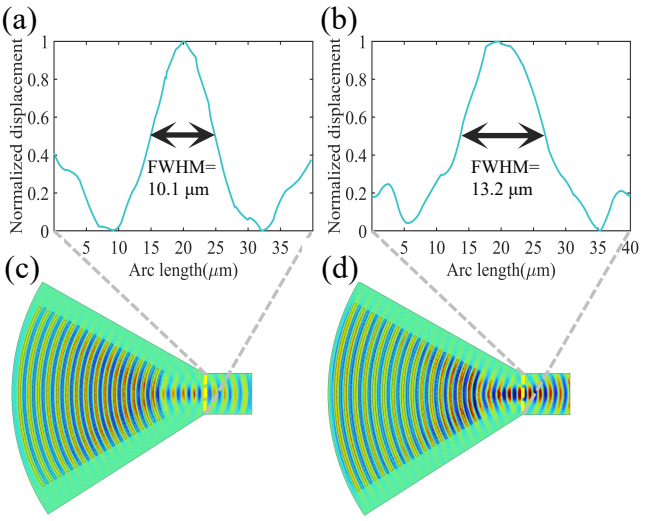

Fig. 2. (a) Displacement along the cross-line of Gaussian IDT. (b) Displacement along the cross-line of circular IDT. (c) Out of plane displacement for Gaussian IDT. (d) Out of plane displacement for circular IDT.

interdigital transducer (IDT). The curvature of focusing type IDT is designed based on the wavefront of gaussian beams, the first electrode finger starts at 5 wavelengths from the focal point, which is shown in Fig. 1(c) and satisfy the following equations:

$$\begin{aligned} w(z) &= w_0\sqrt{1+\left(\frac{z}{z_R}\right)^2} \\ R(z) &= z\left(1+\left(\frac{z_R}{z}\right)^2\right) \\ \theta &= \frac{\lambda}{\pi\omega_0} \end{aligned} \tag{1}$$

w here is the beam width in transverse direction. R is curvature radius of wavefront. w_0 is the beam waist, z_R is Rayleigh length defines the distance over which the beam can propagate without significant divergence. z_R can be expressed as $z_{\mathrm{R}} = \frac{\pi w_0^2}{\lambda}$.

With the same divergence angle and 10 μm wavelength, comparison of circular IDT and Gaussian IDT focusing capability is analyzed by FEA simulation. The width of electrode is 2.5 μm with 15 pairs fingers. The beam waist of the focused beam for Gaussian focusing IDT is designed to 5 μm, which is equal to half wavelength. The bottom electrode was set to floating potential, the focused IDT is excited by oscillating voltage applied at resonant frequency between the fingers of the interfingered electrodes. The out of plane displacement is illustrated in Fig. 2(c) and Fig. 2(d). Focusing capability is evaluated at focal point on surface, displacement along the cross-line is depicted in Fig. 2(a) and Fig. 2(b). Both two types of IDTs exhibit Gaussian-like focusing characteristic. Smaller focusing widths of 10.1 μm is achieved by Gaussian IDT, while 13.2 μm achieved by circular electrodes.

As Gaussian IDT demonstrates better focusing performance for the same divergence angle, the Gaussian IDT is used for all of the ensuing analysis. Thickness field excitation (TFE) and lateral field excitation (LFE) are compared. LFE and TFE transducer have distinct characteristics. LFE design primarily features a parallel configuration of electrodes which is optimal for applications requiring uniform electric fields and is often employed in sensors and capacitive systems. TFE design, on the other hand, involves electrodes that are perpendicular to each other, making it suitable for stimulating thickness mode. Both LFE and TFE are crucial in varied fields, leveraging their specific configurations to fit the demands of different applications.The configurations can be seen in Fig. 3(a) and Fig. 3(c). The electric potentials in two electrical configurations are shown in Fig. 3(b) and Fig. 3(d). In TFE configuration, the electrical field is applied perpendicular to

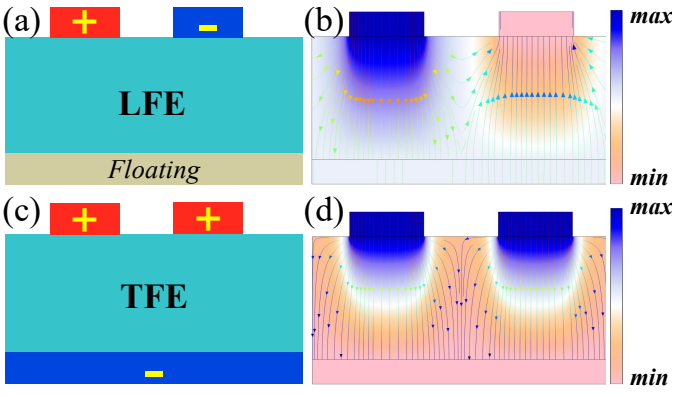

Fig. 3. (a) Electrical excitation method of LFE. (b) Electric potential distribution of LFE. (c) Electrical excitation method of TFE. (d) Electric potential distribution of TFE.

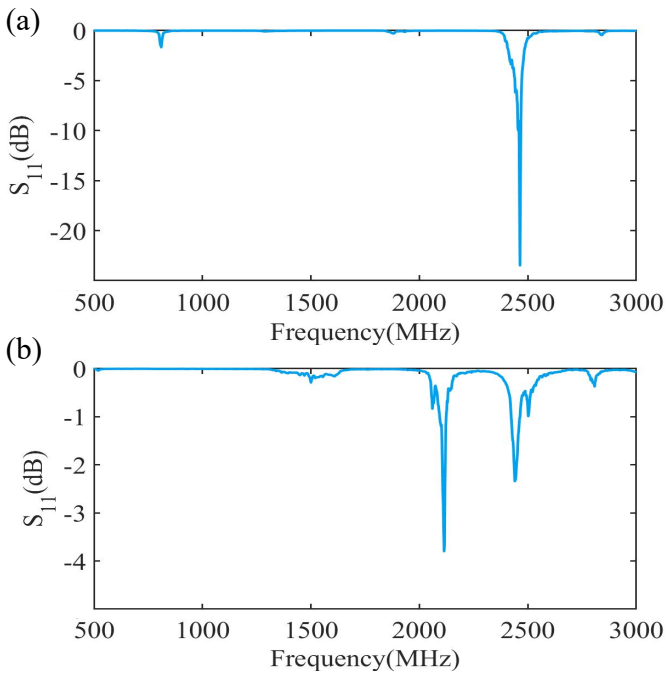

Fig. 4. (a) Simulated S_{11} for LFE Gaussian focusing transducer. (b) Simulated S_{11} for TFE Gaussian focusing transducer.

the surface of the piezoelectric thin film, penetrating through the thickness direction. While in the LFE configuration, in addition to the vertical electric field guided by floating bottom electrodes, the transverse electric field between fingers also exists.

Frequency responses of one port transducers in LFE and TFE configuration are simulated and depicted in Fig. 4(a) and Fig. 4(b) respectively. Through numerical modeling and computational analysis, resonance frequencies and frequency-dependent behaviors of the transducers are explored. LFE one port device shows resonant peak around 834 MHz and 2.46 GHz, which corresponds to S0 and thickness mode respectively. TFE one port device shows resonant peak around 1.51 GHz, 2.13 GHz and 2.46 GHz which corresponds to S0, S1 and thickness mode respectively.

III. Fabrication and Measurements

The fabrication process shown in Fig. 5 starts on a 4 inch high-resistive silicon wafer. First, 10 nm Ti/100 nm Pt is deposited using E-beam evaporation and patterned by lift-off process. Then, 1 µm AlN is deposited utilizing EVATEC CLUSTERLINE® 200 MSQ multi-source system. Vias are wet etched by 85% phosphoric acid. 2 µm SiO_2 is deposited by plasma enhanced chemical vapor deposition (PECVD) and patterned as a hard mask. Following this, 1 µm AlN is etched through by inductively coupled plasma (ICP) etching to define release window. Next, the hard mask is removed, 10 nm Ti/100 nm Pt is deposited utilizing physical vapor deposition (PVD) and patterned by lift-off process. Finally, 200 nm aluminum

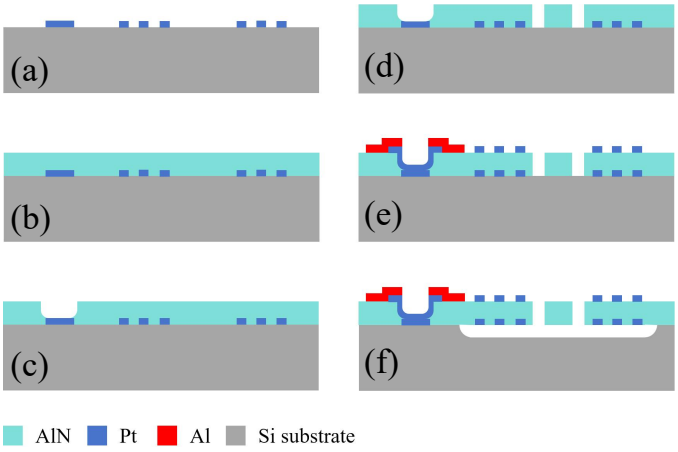

Fig. 5. Process flow of the fabricated Gaussian focusing transducers. (a) Pt bottom electrodes patterned. (b) AlN deposited. (c) AlN wet etched for via. (d) AlN patterned to define release trenches. (e) Top and pad electrodes patterned. (f) The device is suspended by XeF_2 dry etching.

pad layer is defined by lift-off process and the device is released by XeF_2.

Optical microscope photographs and scanning electron microscope photographs of one port tansducers and two port ADLs are provided in Fig. 6. The two port ADLs are consist of identical transmitting and receiving focusing transducers which following the design in previous section, a suspended straight waveguide connects two parts. The width of the waveguide is 10 µm equals to wavelength with lengths varying from 10 µm, 20 µm and 50 µm.

Frequency response of the two-port delay line is characterized by Keysight PNA-L N5234B network analyzer with 200 µm pitch RF probe. According to the measurement results presented in Fig. 7, the LFE-type transducer efficiently stimulates the S0 mode and couples the acoustic wave into the

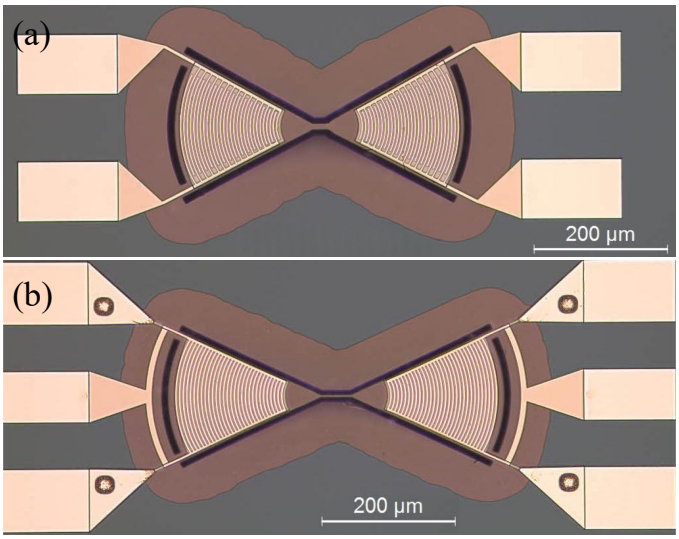

Fig. 6. Optical microscope photographs of (a) two port LFE Gaussian focusing ADL and (b) TFE Gaussian focusing ADL.

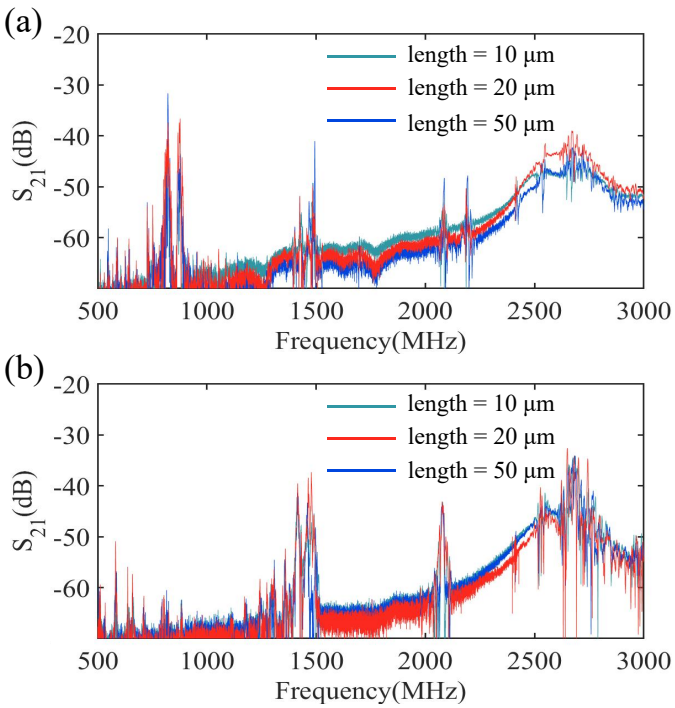

Fig. 7. (a) Measured S_{21} for LFE Gaussian focusing transducer with straight waveguide lengths varying from 10 μm, 20 μm and 50 μm. (b) Measured S_{21} for TFE Gaussian focusing transducer with straight waveguide lengths varying from 10 μm, 20 μm and 50 μm.

wavelength-scale waveguide, achieving a measured insertion loss of 32.16 dB at 824.13 MHz. The high efficiency of the LFE-type transducer in generating the S0 mode is indicative of its potential for applications where low insertion loss is critical. Conversely, the TFE-type transducer was observed to stimulate the A1 mode, with a measured insertion loss of 35.7 dB at 1512.64 MHz. The capability of the TFE-type transducer to effectively stimulate the A1 mode, despite the higher insertion loss compared to the LFE-type transducer, highlights its suitability for different operational regimes where the A1 mode's characteristics are desirable. These results reveal the distinct performance characteristics of the LFE and TFE transducers in the context of frequency response and insertion loss, providing valuable insights into their respective applications in PnIC.

IV. Conclusion

The gaussian lamb wave focusing transducers with different electrical configuration are designed and fabricated. Simulation results illustrate the transducer can produce the expected focused gaussian lamb beam with a beam waist of 5 μm. Smaller focusing widths can be achieved in the same divergence angle compared to circular electrodes. Different frequency responses in TFE and LFE are explored. LFE one port device shows resonant peak around 824.13 MHz and 2.46 GHz. The corresponding two-port ADL show the insertion loss of 32.16 dB at 824.13 MHz. TFE one port device shows resonant peak around 1.51 GHz, 2.13 GHz and 2.46 GHz. The corresponding two-port ADL show the insertion loss of 35.7 dB at 1512.64 MHz, which proves the efficient electromechanical transduction capability of the transducer. The unique properties of these Gaussian Lamb wave focusing transducers make them an excellent candidate for enhancing the performance and functionality of PnICs, particularly in areas where precise control of wave propagation and efficient energy coupling are critical.

Acknowledgment

This work was supported in part by the Natural Science Foundation of Shanghai (23ZR1442400), in part by Jiangsu Provincial Key Research and Development program (BE2023048), in part by the Foundation of the state key laboratory of Transducer Technology (No. SKT2303). The authors also appreciate the device fabrication support from ShanghaiTech Material Device Laboratory (SMDL) and Soft Matter Nanofab (SMN180827).

References

[1] M. Kurosu, D. Hatanaka, K. Onomitsu, and H. Yamaguchi, "On-chip temporal focusing of elastic waves in a phononic crystal waveguide," *Nature Communications*, vol. 9, no. 1, p. 1331, 2018.

[2] W. Bogaerts, D. Pérez, J. Capmany, D. A. B. Miller, J. Poon, D. Englund, F. Morichetti, and A. Melloni, "Programmable photonic circuits," *Nature*, vol. 586, no. 7828, pp. 207–216, 2020.

[3] M. Bicer, S. Valle, J. Brown, M. Kuball, and K. C. Balram, "Gallium nitride phononic integrated circuits platform for GHz frequency acoustic wave devices," *Applied Physics Letters*, vol. 120, no. 24, p. 243502, 2022.

[4] J. Guida, R. Tetro, M. Rinaldi, and S. Ghosh, "Focused S0 Lamb Modes for Gigahertz Delay Lines in 30% Scandium Aluminum Nitride," in *2023 IEEE International Ultrasonics Symposium (IUS)*. Montreal, QC, Canada: IEEE, 2023, pp. 1–4.

[5] D. Lee, Q. Liu, L. Zheng, X. Ma, H. Li, M. Li, and K. Lai, "Direct Visualization of Gigahertz Acoustic Wave Propagation in Suspended Phononic Circuits," *Physical Review Applied*, vol. 16, no. 3, p. 034047, 2021.

[6] A. Siddiqui, R. H. Olsson, and M. Eichenfield, "Lamb Wave Focusing Transducer for Efficient Coupling to Wavelength-Scale Structures in Thin Piezoelectric Films," *Journal of Microelectromechanical Systems*, vol. 27, no. 6, pp. 1054–1070, 2018.

[7] A. Zivari, R. Stockill, N. Fiaschi, and S. Gröblacher, "Non-classical mechanical states guided in a phononic waveguide," *Nature Physics*, vol. 18, no. 7, pp. 789–793, 2022.

[8] W. Fu, Z. Shen, Y. Xu, C.-L. Zou, R. Cheng, X. Han, and H. X. Tang, "Phononic integrated circuitry and spin–orbit interaction of phonons," *Nature Communications*, vol. 10, no. 1, p. 2743, 2019.

[9] J. Guida, R. Tetro, M. Rinaldi, and S. Ghosh, "Compact Bends and Low-Loss Junctions for S0 Lamb Modes in Fully Etched Scandium Aluminum Nitride Acoustic Waveguides," in *2024 IEEE 37th International Conference on Micro Electro Mechanical Systems (MEMS)*. Austin, TX, USA: IEEE, 2024, pp. 1091–1094.

[10] M. Bicer and K. C. Balram, "Low-loss GHz frequency phononic integrated circuits in Gallium Nitride for compact radio-frequency acoustic wave devices." *IEEE Transactions on Ultrasonics, Ferroelectrics, and Frequency Control*, pp. 1–1, 2023.